applied optics

Rapid and automatic 3D body measurement system based on a GPU–Steger line detector

Xingjian Liu,[1,3] Hengshuang Zhao,[4] Guomin Zhan,[1] Kai Zhong,[1] Zhongwei Li,[1,2,*] Yuhjin Chao,[3] and Yusheng Shi[1]

[1]State Key Laboratory of Material Processing and Die & Mould Technology, Huazhong University of Science and Technology, Wuhan, China
[2]Research Institute of Huazhong University of Science and Technology at Shenzhen, Shenzhen, China
[3]Department of Mechanical Engineering, University of South Carolina, Columbia, South Carolina 29208, USA
[4]Department of Computer Science and Engineering, The Chinese University of Hong Kong, Shatin, New Territories, Hong Kong SAR, China
*Corresponding author: zwli@hust.edu.cn

Received 2 May 2016; revised 18 June 2016; accepted 18 June 2016; posted 20 June 2016 (Doc. ID 264417); published 12 July 2016

This paper proposes a rapid and automatic measurement system to acquire a 3D shape of a human body. A flexible calibration method was developed to decrease the complexity in system calibration. To reduce the computation cost, a GPU–Steger line detector was proposed to more rapidly detect the center of the laser pattern and at subpixel level. The processing time of line detection is significantly shortened by the GPU–Steger line detector, which can be over 110 times faster than that by CPU. The key technologies are introduced, and the experimental results are presented in this paper to illustrate the performance of the proposed system. The system can be used to measure human body surfaces with nonuniform reflectance such as hair, skin, and clothes with rich texture.

OCIS codes: (150.6910) Three-dimensional sensing; (150.1488) Calibration; (150.1135) Algorithms; (120.6660) Surface measurements, roughness.

http://dx.doi.org/10.1364/AO.55.005539

1. INTRODUCTION

Extracting various information from the human body plays a significant role in many applications such as 3D printing, customized clothing production, and ergonomics. In the past 20 years, many 3D measurement methods [1–5] have been developed to acquire high-quality 3D body surface data. Among these 3D measurement methods, a very well investigated group of algorithms employs one camera or multiple cameras in order to obtain depth from matching corresponding features. Due to typical correspondence problems that occur in the presence of uniformly colored regions, controllable illumination called structured light, which creates easily detectable features, is often used for accurate and reliable matching during measurement.

Typically, the structured light methods can be classified into two types, i.e., pattern projection [1] and triangulation laser scanning [2]. As for pattern projection method, it is well known for surface properties. Single or multiple coded patterns are projected onto the object, and corresponding features can be determined precisely by decoding the images. Among coding strategies, phase measurement profilometry (PMP) [6] is credited with high spatial resolution capability, and it is very popular in surface geometric dimension quality evaluation [4,7–9]. The PMP method needs fewer images than that required in laser scanning system, and its measurement time can be reduced to several milliseconds. But there still exist challenging problems that need to be solved for accurate 3D measurements. Generally the PMP method is based on the analysis of the diffusion component of an active illumination, so that the results are sensitive to the texture and reflectance of measured surfaces. Aiming at solving these problems, many methods (including auto-exposure time [10], modulated phase-shifting [11], diffused structured light [12], micro-phase shifting [13], and others) have been proposed. But they can only improve the quality of the results to some extent. Currently the most prevailing solution is surface coating of micro-white powders, which will make the surface exhibit Lambertian reflectance. However, for measuring a human body, it is impossible to spray micro-white powder. The hair, skin, and color clothes will make the measurements more difficult for acquiring high-quality results while they will exhibit different reflectance. For instance, the light color surfaces have higher reflectance ratio than dark ones. Thus, it is usually difficult to configure the measurement system to measure surfaces with nonuniform reflectance.

As for the triangulation laser scanning method [2], single or multiple lines are projected onto the object surface to be measured, and they are imaged by one or two cameras. By extracting the lines in the images, 3D shape of the lines can be reconstructed by the optical triangulation method. As the

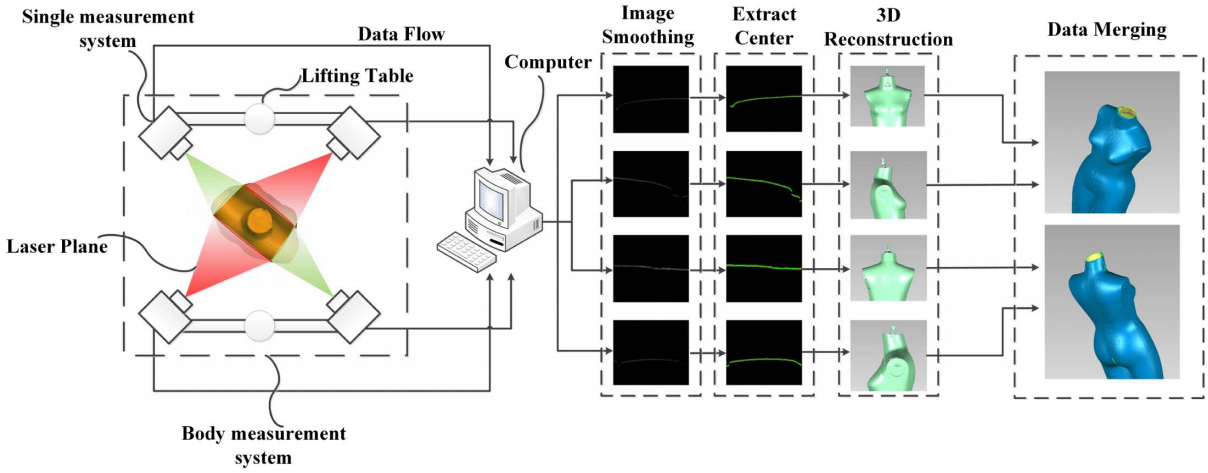

Fig. 1. Scanning procedure of the 3D body measurement system.

laser scans across the object, the 3D shape can then be obtained [5]. Compared with the PMP method [6], the major advantage of the triangulation laser scanning method is that it is insensitive to the color of the measured objects to some extent. Due to this point, the triangulation laser scanning method has been widely used in applications when surface coating of micro-white powder is prohibited, such as industrial 3D inspection [14] and digital protection of cultural relics [15]. Therefore, a triangulation laser scanning method is more suitable for 3D body measurement. However, the measurement time becomes another concern while using this method because it is difficult for a person to keep standing motionless for a long time. Therefore, it is valuable in improving the speed of the measurement and calculation efficiency in applying the triangulation laser scanning method.

For a typical triangulation laser scanning system, accurate line center detection is the most time-consuming procedure in realizing triangulation reconstruction. At the same time, the detection precision dominates the reconstruction precision once the system mechanism has been determined. Several approaches for line detection have been proposed since 1986 [16–21]. The algorithms are reviewed in detail in [22]. Among these approaches, the unbiased line detection algorithm proposed by Steger [18,22] can achieve subpixel precision detection and has outstanding noise robustness performance. It corrects the bias in line position, which is often introduced by other algorithms when the two sides of a line have different contrast. It has been widely applied to triangulation laser scanning [23–25]. However, there is a large number of convolution and other calculations in Steger's algorithm, which reduces computational efficiency.

To realize rapid and automatic measurement of a 3D human body, this paper presents a measurement system that can acquire a 3D shape of a human body in a flexible posture. As shown in Figs. 1 and 2, laser generators and cameras are all fixed on two lift tables. As the lift tables go down synchronously with a step of 0.5 to 2 mm, the 3D body is quickly scanned from head to foot. At the same time, multiple laser generators are used to project laser lines from different directions, and multiple CCD cameras capture the laser line images.

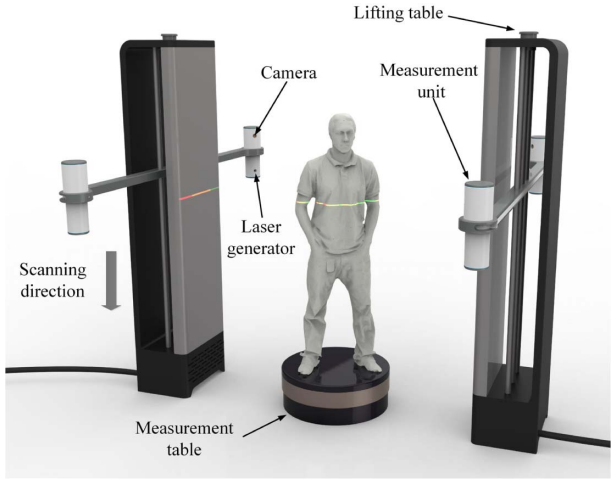

Fig. 2. 3D body measurement system.

Then the line centers are detected at subpixel level, and the 3D points are reconstructed by triangulation method. For this system, many parameters need to be calibrated. Usually, different calibration methods and types of the calibration targets (planar or 3D) are conducted. To simplify the calibration procedure, a flexible calibration method, which only needs a planar target, is proposed. By using this planar target, all the parameters of the system can be obtained, including the cameras' intrinsic parameters, laser plane equations, scanning directions, and position transformation relationships. A precision assessment experiment verified that the measurement precision can reach within 1 mm by conducting the proposed calibration method. A GPU–Steger line detector is implemented to accelerate the line detection process. A hybrid parallel computing architecture is proposed, which combines the advantages of a CPU (logical control) and GPU (parallel mathematics operations). To fully utilize the powerful parallel computation capability of a GPU, we designed a 3D grid and 3D block parallel structure for calculation. The experiments demonstrate that computation speed by using a GPU (NVidia GTX TITAN X) can be over

110 times faster than that by CPU (Inter i7 3770, 3.4 GHZ). The key technologies are introduced, and the experimental results are presented to illustrate the performance of the method. The proposed system can be used to measure human body surfaces with nonuniform reflectance such as hair, skin, and clothes with rich texture.

This paper is organized as follows. Section 2 presents the laser vision principle and the proposed flexible calibration method. Section 3 explains the principle of Steger algorithm and its hybrid parallel computing architecture. Section 4 shows experimental results, including the calibration, precision assessment, the parallel computing tests and measurement to illustrate the performance of this system. Finally, a discussion on the noise is given. Section 5 summarizes the paper.

2. SYSTEM PRINCIPLE AND CALIBRATION

A. Principle of Triangulation Laser Scanning

The triangulation laser scanning system mainly contains a laser line generator and one or two cameras. In our method only one camera is used. As shown in Fig. 3, during the measurement the laser line generator projects a laser plane in space and forms a distorted line on the surface of object while the camera captures the laser line image correspondingly. Then the laser line can be extracted. For an arbitrary point p on the line, we can find a space line by connecting point p with the optical center O_c. The space line intersects with the laser plane at the measured point P. All the points on the laser line can then be reconstructed. In this way, as the laser vision system scanning the entire object, the profile of object can be obtained.

In this paper, a 2D image point is denoted by $\mathbf{p} = [u, v]^T$, and A 3D point is denoted by $\mathbf{P} = [X, Y, Z]^T$. We use $\widetilde{\mathbf{p}}$ to denote the augmented vector by adding 1 as the last element: $\widetilde{\mathbf{p}} = [u, v, 1]^T$ and $\widetilde{\mathbf{P}} = [X, Y, Z, 1]^T$. And s is an arbitrary scale factor. The camera is modeled by the pinhole model. The relationship between a 3D point and its image point from a pinhole model is given by

$$s\widetilde{\mathbf{p}} = \mathbf{A}[\mathbf{R} \quad \mathbf{T}]\widetilde{\mathbf{P}}, \quad \text{with } \mathbf{A} = \begin{bmatrix} f_x & \gamma & u_0 & 0 \\ 0 & f_y & v_0 & 0 \\ 0 & 0 & 1 & 0 \end{bmatrix}. \tag{1}$$

Here $\mathbf{R}$ and $\mathbf{T}$, called the extrinsic parameters, are the rotation and translation matrices, which relate the world coordinate system to the imaging coordinate system. $\mathbf{A}$ is called the camera intrinsic matrix, with (u_0, v_0) the coordinates of the principal point, f_x and f_y the scale factors in the image u and v axes (camera focal lengths), γ the parameter describing the skew of the two image axes.

The equation of the laser plane is $A_L x + B_L y + C_L z + D_L = 0$, and the 3D point $\mathbf{P}$ is located in the plane. Combining this equation with Eq. (1), one gets

$$\begin{cases} s\widetilde{\mathbf{p}} = \begin{bmatrix} f_x & \gamma & u_0 & 0 \\ 0 & f_y & v_0 & 0 \\ 0 & 0 & 1 & 0 \end{bmatrix} [\mathbf{R} \quad \mathbf{T}]\widetilde{\mathbf{P}} \\ [A_L, B_L, C_L, D_L]\widetilde{\mathbf{P}} = 0 \end{cases}. \tag{2}$$

If the image point $\mathbf{p}$, the camera parameters $\mathbf{A}$, the extrinsic parameters $\mathbf{R}$, $\mathbf{T}$ and the laser plane's equation A_L, B_L, C_L, D_L are known, the 3D point value $\mathbf{P}$ can be determined.

From the above discussion, one can get single line 3D data from a single measurement. For a 3D object, as the laser scans across the object, many line data are obtained and then need to be merged together. As shown in Fig. 4, a measurement system scans over the surface of the object with the step D. Suppose the coordinate at the lower position is (X_L, Y_L, Z_L) and at the next position the coordinate is (X_U, Y_U, Z_U). The relationship between the two coordinates is calculated by

$$(X_U, Y_U, Z_U) = (X_L + \Delta X, Y_L + \Delta Y, Z_L + \Delta Z), \tag{3}$$

where ΔX, ΔY, ΔZ are the projected components of step D in the camera coordinate system.

B. Flexible Calibration Method

Before implementing the triangulation laser scanning discussed in the previous section, we need to calibrate some parameters, including the cameras' intrinsic parameters, laser plane equations, scanning directions, and position transformation relationships. There are different calibration methods and types of calibration targets used to calibrate the whole system. It is a tedious step in the process of the entire measurement implementation. In order to decrease the complexity of this process, a flexible calibration method is proposed. Compared with

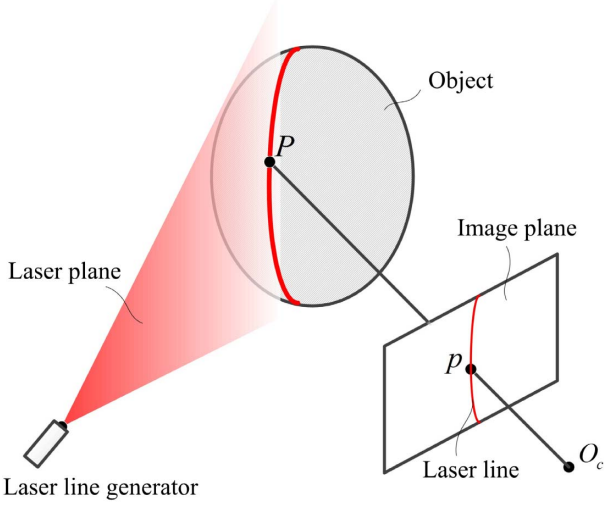

Fig. 3. Principle of triangulation laser scanning.

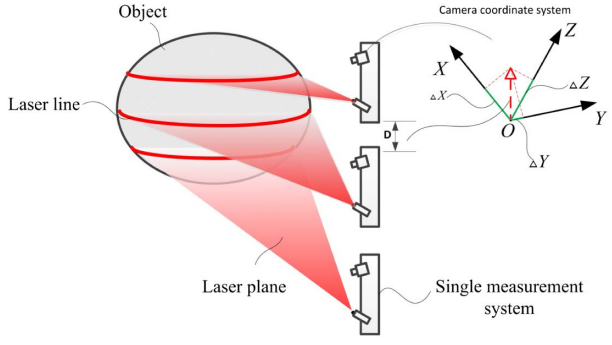

Fig. 4. Principle of data merging.

traditional methods, which often need a 3D target, our method only requires a flat 2D pattern as the calibration target. First, we use the classic 2D target calibration method [26] to calibrate the intrinsic parameters **A** in Eq. (1) of the four cameras. Then we calibrate the others.

1. Laser Plane Calibration

As shown in Fig. 5, a laser line is projected onto the calibration target and captures the scene. The points of the laser line center can be detected by the method discussed in Section 3. These laser line center points and the optic center O_c constitute a plane, which is called the object plane. According to the intrinsic calibration results, one can calculate the equation of the object plane:

$$A_o x + B_o y + C_o z + D_o = 0. \tag{4}$$

The center points of the circles on the calibration target can then be detected in subpixels. While the intrinsic parameters are known, the value of the center points in the camera coordinate can be obtained. Then the target plane equation can be fitted from the points:

$$A_t x + B_t y + C_t z + D_t = 0. \tag{5}$$

The two planes intersect, and one can get N crossing points $P_{11}, P_{12}, \ldots, P_{1N}$. These points are all in the laser plane. Then we can move the target and get another group of points. Finally, we can obtain M groups of crossing points:

$$\{P_{11}, P_{12}, \ldots, P_{1N}, P_{21}, P_{22}, \ldots, P_{2N}, P_{M1}, P_{M2}, \ldots, P_{MN}\}.$$

Stacking the points, they can be written as a matrix $\mathbf{K} \in \mathbb{R}^{(M*N)\times 4}$. For a single triangulation laser scanning system, the laser plane equation is $A_L x + B_L y + C_L z + D_L = 0$. The overdetermined Eq. (6) can be obtained. The least-squares method is used to fit the laser plane:

$$\mathbf{KH} = \mathbf{0} \quad \text{where } \mathbf{H} = [A_L, B_L, C_L, D_L]. \tag{6}$$

2. Scanning Direction Calibration

After calibrating the laser plane, one needs to calibrate the scanning direction equation. As Fig. 6 shows, an image of the calibration target is taken at the lowest place. The coordinates of the circles are obtained in the camera sensor coordinate system. Then the lifting table moves up. After moving a distance of d, it stops and captures a second image. The lifting table travels N positions along its way to capture the entire object. We define $x_{i,j}$ as the x coordinate of jth circle on ith target image, and Δx_i as the mean value of x coordinate on the ith target image:

$$\Delta x_i = \frac{(x_{i+1,1} - x_{i,1}) + (x_{i+1,2} - x_{i,2}) + \ldots + (x_{i+1,K} - x_{i,K})}{K},$$
$$\Delta y_i = \frac{(y_{i+1,1} - y_{i,1}) + (y_{i+1,2} - y_{i,2}) + \ldots + (y_{i+1,K} - y_{i,K})}{K},$$
$$\Delta z_i = \frac{(z_{i+1,1} - z_{i,1}) + (z_{i+1,2} - z_{i,2}) + \ldots + (z_{i+1,K} - z_{i,K})}{K}, \tag{7}$$

where $i = 1, 2, \ldots, N-1$, and K is the number of the circles. Assuming $\Delta\bar{x}$ is the mean value of Δx_i, then one can get the unit increment D_x on the x coordinate and the same principal for D_y and D_z:

$$D_x = \frac{\Delta\bar{x}}{d}; \qquad D_y = \frac{\Delta\bar{y}}{d}; \qquad D_z = \frac{\Delta\bar{z}}{d}. \tag{8}$$

3. Position Transformation Calibration

The position transformation between the four cameras is then calibrated. As shown in Fig. 7, the coordinate system 1 is regarded as the reference coordinate system. We need to calibrate three position relationships that are relative to the reference. The position transformation between camera 1 and camera 2 is calibrated at first. The images of the calibration target are captured by the two cameras correspondingly. Then the position transform ($\mathbf{R_{12}}$, $\mathbf{T_{12}}$), as shown in Eq. (9), can be estimated by solving the perspective-n-point problem (PnP problem) [27]. The rest ($\mathbf{R_{23}}$, $\mathbf{T_{23}}$, $\mathbf{R_{34}}$, $\mathbf{T_{34}}$) can be done in the same manner:

$$\mathbf{R_{12}}\begin{bmatrix} x_2 \\ y_2 \\ z_2 \end{bmatrix} + \mathbf{T_{12}} = \begin{bmatrix} x_1 \\ y_1 \\ z_1 \end{bmatrix}. \tag{9}$$

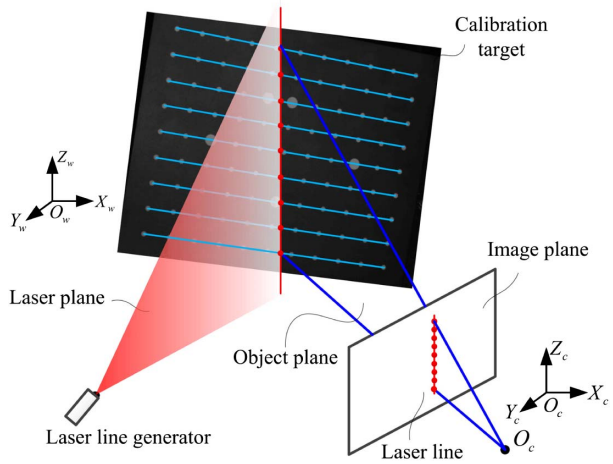

Fig. 5. Calibration of laser plane.

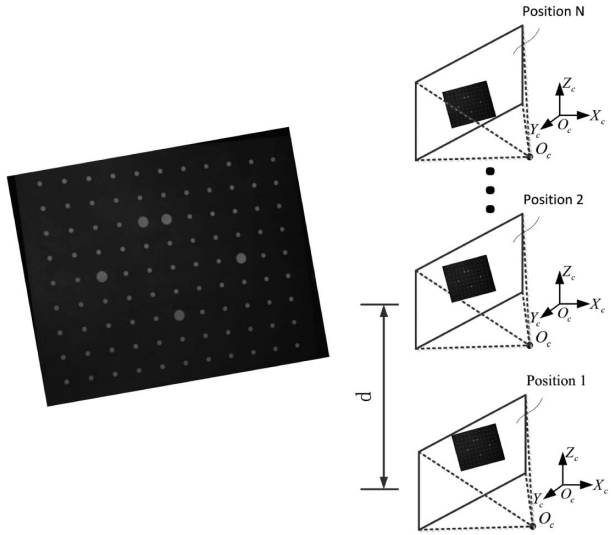

Fig. 6. Calibration of scanning direction equation.

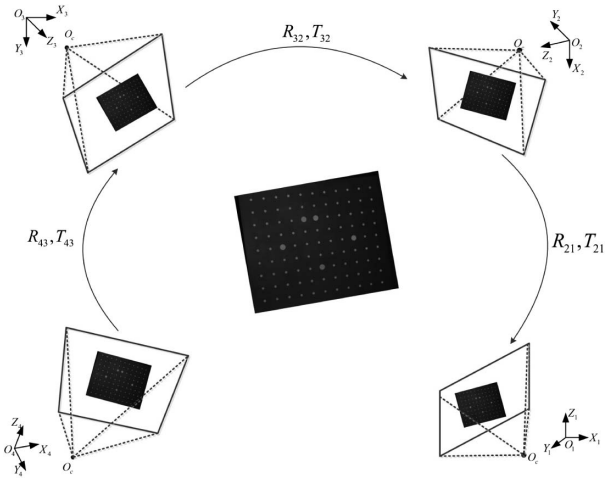

Fig. 7. Calibration of position relationships between the four cameras.

3. GPU-BASED STEGER LINE DETECTOR

A. Principle of Steger Algorithm

Given the line model discussed in [22], for image of a projected laser line, the Gaussian profile is a better fit than the parabolic profile. Thus, the asymmetric Gaussian is chosen in our method. A second alternative is the asymmetric Gaussian line profile of width w and asymmetry $a \in [0, 1]$:

$$f_g(x) = \begin{cases} e^{-\frac{x^2}{2w^2}}, & x \le 0 \\ a + (1-a)e^{-\frac{x^2}{2w^2}} & x > 0 \end{cases}. \tag{10}$$

The idea is most easily illustrated in one dimension, as discussed in [22]. Rather than simply checking where the values of the derivative is zero or goes from positive to negative between neighboring pixels, a second-order Taylor polynomial is used to estimate the value of the "image function." Here we define r, r', r'' as the functions that are obtained when convolving with the Gauss kernel and its derivatives; the Taylor polynomial can be obtained by $p(x) = r + r'x + \frac{1}{2}r''x^2$. If $p'(x) = 0$, one gets $p'(x) = r' + r''x$, and thus $p(x) = -\frac{r'}{r''}$. The subpixel location for each line point is detected.

In two dimensions, the same idea can be applied. But the direction of the line in each pixel cannot be gained, so it is difficult to calculate the derivative in the direction perpendicular to the line. As such, the Hessian matrix [28], which contains all of the second derivatives of r with respect to the image coordinates $f(x, y)$, is calculated instead:

$$H(x,y) = \begin{bmatrix} \frac{\partial^2 g(x,y)}{\partial x^2} & \frac{\partial^2 g(x,y)}{\partial x \partial y} \\ \frac{\partial^2 g(x,y)}{\partial y \partial x} & \frac{\partial^2 g(x,y)}{\partial y^2} \end{bmatrix} \otimes f(x,y) = \begin{bmatrix} r_{xx} & r_{xy} \\ r_{yx} & r_{yy} \end{bmatrix}. \tag{11}$$

Here $g(x, y)$ is the Gaussian kernel. The direction perpendicular to the line can be determined by finding the eigenvectors and eigenvalues of the matrix. Given the longest eigenvector $n = (n_x, n_y)$, the point can be obtained by inserting $t(n_x, n_y)$ into the Taylor polynomial, and setting its derivative along t to zero. Hence, the point is given by $p = (p_x, p_y) = tn = t(n_x, n_y)$, where

$$t = -\frac{n_x r_x + n_y r_y}{n_x^2 r_{xx} + 2n_x n_y r_{xy} + n_y^2 r_{yy}}. \tag{12}$$

Again, $(p_x, p_y) \in [-\frac{1}{2}, \frac{1}{2}] \times [-\frac{1}{2}, \frac{1}{2}]$ is required in order for a point to be declared a line point.

B. Hybrid Parallel Computing Architecture

As the basic principles discussed above, the most time-consuming part when using the Steger algorithm to extract lines in an image is the image 2D convolutional operation. In the Steger algorithm, five times of 2D convolutional operations are needed, which take up time in calculations. In our proposed measurement system, multiple images are collected by four cameras. In order to accelerate the calculation time consumed, GPU implementation for 2D convolution, which processes multiple images simultaneously, is adopted in our system.

Although a GPU is powerful for parallel computing, it cannot take the role of a CPU. A CPU is suitable for fine calculations and logical control, while a GPU is suitable for parallel mathematics operations. Taking these into consideration, a hybrid parallel computing architecture is proposed here. As shown in Fig. 8, the convolutional kernels and images are prepared in a CPU and transmitted to the GPU memory; then image 2D convolution parallel computing and pixel-wise Jacobi matrix decomposition are operated in the GPU host. Finally, the calculated results are transmitted back to the CPU memory.

To fully utilize the power of parallel computation capability of the GPU, a 3D grid and 3D block parallel structure for calculation were designed, as illustrated in Fig. 9. Launching GPU kernel functions cost considerable time. Thus, for the same amount of computation, it is desirable to design a structure that calls the GPU kernel functions less frequently. GPU threads are organized by grid and block. Both the maximum dimensions of grid and block are 3. Thus, in our proposed architecture, per pixel is designed to be processed by one thread, assuming that the 2D image's resolution is W*H, and there are N images to be processed at one time. Then the index of each block and each thread can be determined. The number of threads per processing is girdDim.x*girdDim.y*girdDim.z*blockDim.x*blockDim.y*$blockDim.z$. This result should be no smaller than N*W*H.

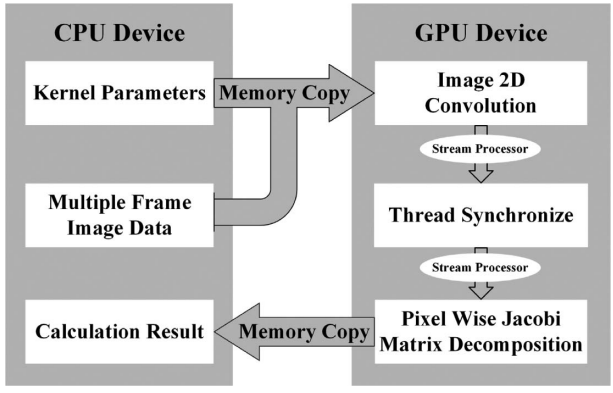

Fig. 8. Hybrid parallel computing architecture.

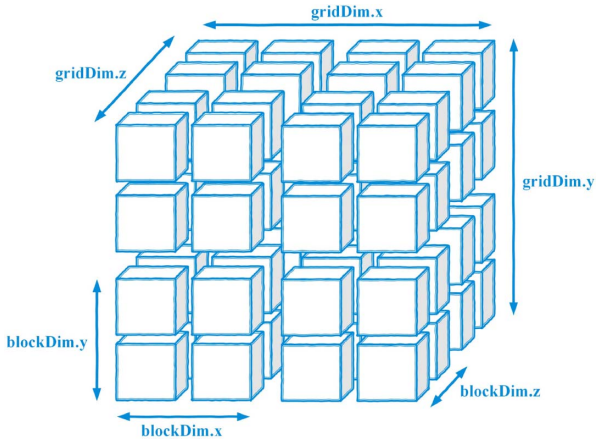

Fig. 9. 3D grid and 3D block GPU architecture.

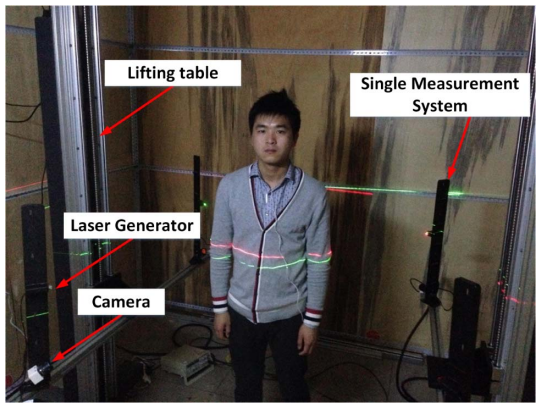

Fig. 10. 3D body measurement system.

4. EXPERIMENTS AND DISCUSSION

As shown in Fig. 10, the performance of the proposed approach was verified with a laser scanning system comprised of four laser generators and four MER-125-30UM CMOS cameras with a Pentax C1614-M lens. The CMOS cameras resolutions are both 1292 × 964. In this system a desktop computer with a NVidia GPU processer is used; its configurations are CPU (Inter Core i7 3770 3.4 GHZ), GPU (NVidia GTX TITAN X), and memory (16 GB).

A. Calibration Results and Precision Assessment

The flexible method stated in the second section is used to calibrate the parameters of the system. The calibration results are shown in Table 1. To test the precision of our system, a standard sphere with sphere center distance of 149.12 mm, as shown in Fig. 11, was used. The results shown in Fig. 11 indicate that the measurement precision can reach within 1 mm.

B. Parallel Computing Tests

The experimental system of Fig. 10 used Microsoft Visual Studio 2013 with managed C++, and GPU parallel computing is implemented on the CUDA platform from NVIDIA Corporation. In CUDA the massive paralleling threads are organized by multiple thread blocks, the massive blocks are organized grid, each block contains multiple threads, and the grid contains multiple blocks. All the threads in one block must be launched to the same stream multiprocessor (SM) in the GPU. Each SM contains eight stream processors (SP), and each thread can be implemented on the SP. In each SM, there may exist multiple active blocks to hide the access delay. In other words, more threads per block can make better use of the GPU hardware resources. On the other hand, the clock rate of SP is typically twice that of SM; during each SM processing cycle, eight SP units can process 16 threads. Therefore, to satisfy the merged global buffer accessing condition, the number of threads per block should be 32 integer times. Also, the number of registers in each block is finite. So in most GPU devices, the maximum number of threads per block is limited to 1024. More threads per block will cause less registers per thread in the block, thus extending the processing time per thread. Less threads per block will cause more blocks in total, thus causing access delay of the blocks in the grid. To properly design the structure of GPU threads per block and blocks per grid in the 3D architecture, we test the average computation time of line detection by using the same number of images with the same resolutions but a different number of blocks and a

Table 1. System Calibration Results

Camera Parameters	**Focal Length (mm): f_x, f_y**	**Principal Point: u_o, v_o**	**Distortion Coefficients: k_1, k_2, g_1, g_2, k_3**
Camera 1	2235.868, 2235.772	634.303, 484.661	−0.086, 0.112, −0.0005, 0.0003, 0
Camera 2	2223.540, 2223.812	626.184, 481.005	−0.111, 0.273, 0.0011, −0.0006, 0
Camera 3	2239.214, 2239.954	642.167, 478.338	−0.097, 0.072, −0.0004, 0.0004, 0
Camera 4	2228.382, 2229.045	627.002, 461.182	−0.101, 0.224, −0.0001, −0.0006, 0
Geometry parameters	**Laser plane: A_L, B_L, C_L, D_L**	**Axis parameter: D_x, D_y, D_z**	
System 1	−0.005, −0.873, 0.487, 283.815	−0.011, 0.886, −0.463	
System 2	−0.028, −0.909, 0.414, 301.950	−0.001, 0.915, −0.402	
System 3	−0.019, −0.891, 0.452, 284.949	−0.014, 0.879, −0.475	
System 4	−0.006, −0.902, 0.431, 280.128	−0.018, 0.889, −0.457	
Position transform	**$R = [\phi_x, \phi_y, \phi_z]$; $T = [t_x, t_y, t_z]$**		
System 1 & System 2	R_{12} = [1.699, −1.212, −1.210]; T_{12} = [693.460, 362.446, 702.753]		
System 2 & System 3	R_{23} = [1.713, −1.130, −1.146]; T_{23} = [804.577, 340.372, 691.434]		
System 3 & System 4	R_{34} = [1.609, −1.125, −1.255]; T_{34} = [764.460, 305.795, 681.875]		

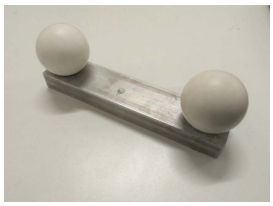

(a) standard ball

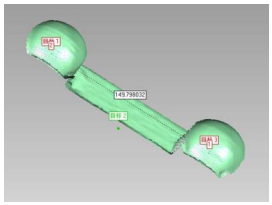

(b) measurement results of the standard ball

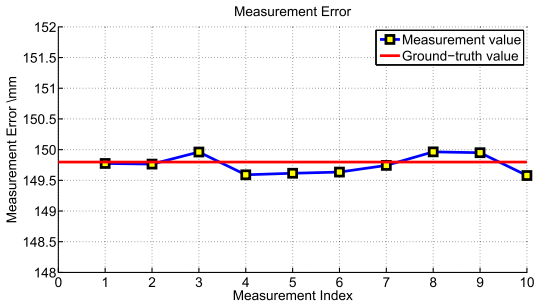

(c) measurement error of the standard ball

Fig. 11. Precision assessment of the measurement system.

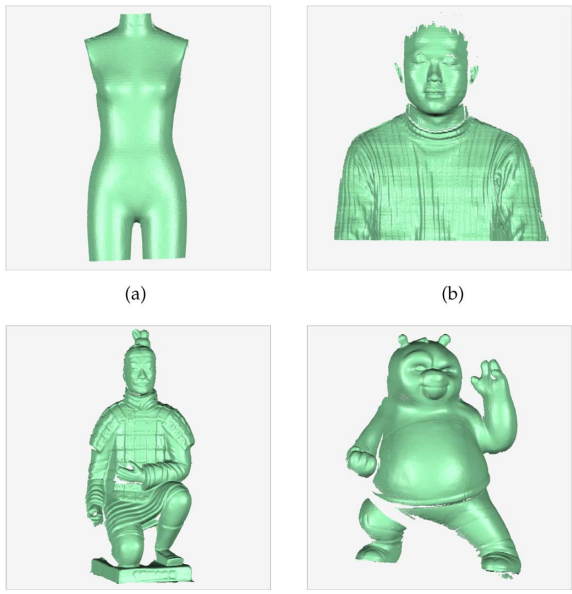

(a) (b) (c) (d)

Fig. 13. Measured point clouds: (a) mannequin; (b) human; (c) statue; (d) panda.

different number of threads per block to harvest the maximum computation power of the GPU.

In our experiment, N, W, and H equal to 640, 1292, and 964 separately. The total number of GPU threads equals to the total number of pixels, which is the product of N, H, and W. Thread number also is decided by the multiplication result of block number and threads per block. So we test different GPU settings in the experiment (different block number and threads per block). The results are shown in Fig. 12. The y axis is arranged by a logarithm function of the number of threads per block on 2, that is, $y = \log 2$ (number of threads per block). When the number of blocks is large, the GPU resources cannot be fully utilized, and the access delay induces more time for calculation. On the contrary, when the number of threads per block is large, the GPU resource for each thread will not be sufficient. Therefore each procedure has its own optimal block number and thread number per block according to its computation characteristics.

In order to illustrate the performance of the GPU-based Steger line detection method, four different objects were measured. The point clouds are shown in Fig. 13, while the image acquisition rate is set to 30 fps, and the exposure time is set to 50 ms. As shown in Fig. 8, the whole system is a hybrid parallel

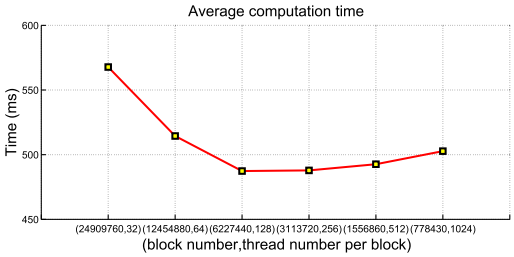

Fig. 12. Average computation times with different GPU settings (number of blocks and number of threads per block).

computing architecture; the CPU is responsible for image data acquisition and result saving; the GPU is responsible for computation, and the whole system is a hybrid utilization. So for the computing part, the comparison should between the proposed GPU strategy and the conventional CPU scheme alone. The corresponding computation times are shown in Table 2. The results indicate that the computation speed in the GPU alone can be over 110 times faster than that in the CPU alone.

C. Measurement Results

To show the robustness to surfaces with nonuniform reflectance, a man's bust and a big Hugo's statue were measured (the results are shown in Fig. 14). The clothes and the hair with rich texture can be measured. Details of the statue also can be acquired with our method. In the experiment, the four scanned point sets are all transformed into a global coordinate system by applying the calibration parameters. However, there are some misalignments caused by the mechanical vibrations and manufacturing errors. The ICP algorithm [29] was used to merge the point clouds together. A box grid filter method [30] was conducted to merge the registered multiple point clouds into a complete point cloud. Points within the same box grid are sampled to a single point, and the grid step is specified as the average point cloud density. The merged point cloud

Table 2. Computation Time Using CPU and GPU Alone

Measured Objects	Points Number	CPU (ms)	GPU (ms)
Mannequin	524,946	90,735	810
Human	551,879	96,451	876
Statue	523,847	89,155	801
Panda	243,099	61,424	548

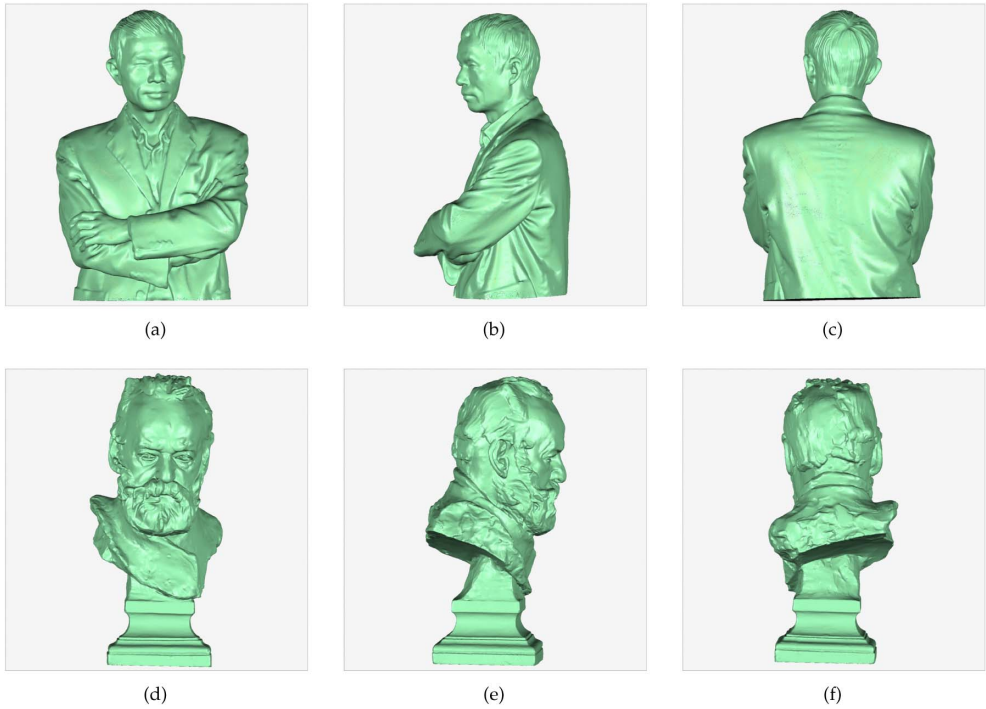

Fig. 14. Measurement results: (a)–(c) a real human; (d)–(f) the Hugo's statue.

preserves the original 3D shape and points of the measured point clouds and also avoid the points redundancy in overlapping regions.

From the measurement results in Figs. 12 and 14, it can be concluded that arbitrary shape can be reliably measured. However, there still exists some low-frequency ripples when the method is applied to measure a real human body, as shown in Figs. 13(b) and 14(a)–14(c). They are mainly caused by the slight motion of the human body. These ripples will be even larger when the motion is faster. Increasing the image acquiring speed can reduce the error to some extent. Because the motion of the human is random, it presents some challenges and will be considered in our future research work. As for the color information, we intend to add a color camera beside each monochrome camera for capturing the color texture. Once the intrinsic and extrinsic parameters of the two cameras are calibrated, the color information can be mapped into the 3D point cloud, and this technique is mature and easy to be implemented.

5. CONCLUSION

In this paper, a rapid and automatic 3D body measurement system is proposed. In this method, multiple laser generators are used to project laser lines from different directions. Multiple CCD cameras capture the laser line images correspondingly, and the 3D points are reconstructed by the triangulation method. To decrease the calibration complexity of the system, a flexible calibration method is presented, which only needs a planar target. The precision assessment experiment verifies that the measurement precision can reach within 1 mm by conducting the proposed calibration method. A GPU-based Steger line detector is developed to extract the center of the laser pattern in the subpixel level. The processing time of the center detector is significantly shortened by the GPU–Steger line detector. The experiments demonstrate that computation speed by using a GPU (NVidia GTX TITAN X) can be over 110 times faster than that by a CPU (Inter i7 3770, 3.4 GHZ). Compared with the prevailing pattern projection methods, it can measure human body surfaces with nonuniform reflectance such as hair, skin, and clothes with rich texture. In our future work, we will concentrate on decreasing the low-frequency noises that are caused by slight motion of the human body and the color information merging to raise the quality of the 3D data.

Funding. National Natural Science Foundation of China (NSFC) (51505169); Science and Technology Planning Project of ShenZhen, China (JCYJ20050630155150209); China Scholarship Council (CSC) (201506160001).

Acknowledgment. Support provided by the China Scholarship Council (CSC) during a visit of Xingjian Liu to the University of South Carolina is acknowledged. We thank Weitao Zheng and Hao Jiang for the help in building the system hardware platform.

REFERENCES

1. F. Chen, G. M. Brown, and M. Song, "Overview of three-dimensional shape measurement using optical methods," Opt. Eng. **39**, 10–22 (2000).
2. F. Blais, "Review of 20 years of range sensor development," J. Electron. Imaging **13**, 231–243 (2004).
3. S. C. Park and M. Chang, "Reverse engineering with a structured light system," Comput. Ind. Eng. **57**, 1377–1384 (2009).

4. D. Hong, H. Lee, M. Y. Kim, H. Cho, and J. I. Moon, "Sensor fusion of phase measuring profilometry and stereo vision for three-dimensional inspection of electronic components assembled on printed circuit boards," Appl. Opt. **48**, 4158–4169 (2009).
5. Y.-C. Zhang, J.-X. Han, X.-B. Fu, and H.-B. Lin, "An online measurement method based on line laser scanning for large forgings," Int. J. Adv. Manuf. Technol. **70**, 439–448 (2014).
6. S. Zhang, "Recent progresses on real-time 3D shape measurement using digital fringe projection techniques," Opt. Lasers Eng. **48**, 149–158 (2010).
7. K. Zhong, Z. Li, Y. Shi, C. Wang, and Y. Lei, "Fast phase measurement profilometry for arbitrary shape objects without phase unwrapping," Opt. Lasers Eng. **51**, 1213–1222 (2013).
8. Z. Li, K. Zhong, Y. F. Li, X. Zhou, and Y. Shi, "Multiview phase shifting: a full-resolution and high-speed 3d measurement framework for arbitrary shape dynamic objects," Opt. Lett. **38**, 1389–1391 (2013).
9. K. Zhong, Z. Li, X. Zhou, Y. Li, Y. Shi, and C. Wang, "Enhanced phase measurement profilometry for industrial 3d inspection automation," Int. J. Adv. Manuf. Technol. **76**, 1563–1574 (2015).
10. J. Liang, Y. Qin, and Z. Hong, "An auto-exposure algorithm for detecting high contrast lighting conditions," in *7th International Conference on ASIC (ASICON'07)* (IEEE, 2007), pp. 725–728.
11. D. Liu, G. Hua, P. Viola, and T. Chen, "Integrated feature selection and higher-order spatial feature extraction for object categorization," in *IEEE Conference on Computer Vision and Pattern Recognition (CVPR)* (IEEE, 2008), pp. 1–8.
12. S. K. Nayar and M. Gupta, "Diffuse structured light," in *IEEE International Conference on Computational Photography (ICCP)* (IEEE, 2012), pp. 1–11.
13. M. Gupta and S. K. Nayar, "Micro phase shifting," in *IEEE Conference on Computer Vision and Pattern Recognition (CVPR)* (IEEE, 2012), pp. 813–820.
14. Y. Zhang, S. Wang, X. Zhang, F. Xie, and J. Wang, "Freight train gauge-exceeding detection based on three-dimensional stereo vision measurement," Mach. Vision Appl. **24**, 461–475 (2013).
15. M. Levoy, K. Pulli, B. Curless, S. Rusinkiewicz, D. Koller, L. Pereira, M. Ginzton, S. Anderson, J. Davis, J. Ginsberg, J. Shade, and D. Fulk, "The digital Michelangelo project: 3d scanning of large statues," in *Proceedings of the 27th Annual Conference on Computer Graphics and Interactive Techniques* (ACM/Addison-Wesley, 2000), pp. 131–144.
16. M. Shah, A. Sood, and R. Jain, "Pulse and staircase edge models," Comput. Vision Graphics Image Process. **34**, 321–343 (1986).
17. J.-S. Chen and G. Medioni, "Detection, localization, and estimation of edges," IEEE Trans. Pattern Anal. Mach. Intell. **11**, 191–198 (1989).
18. C. Steger, "An unbiased detector of curvilinear structures," IEEE Trans. Pattern Anal. Mach. Intell. **20**, 113–125 (1998).
19. J. Chen, Y. Sato, and S. Tamura, "Orientation space filtering for multiple orientation line segmentation," IEEE Trans. Pattern Anal. Mach. Intell. **22**, 417–429 (2000).
20. D. Ziou, "Line detection using an optimal IIR filter," Pattern Recognit. **24**, 465–478 (1991).
21. K. Rothaus and X. Jiang, "Multi-scale midline extraction using creaseness," in *Pattern Recognition and Image Analysis* Vol. **3687** of Lecturer Notes in Computer Science (2005), 502–511.
22. C. Steger, "Unbiased extraction of lines with parabolic and Gaussian profiles," Comput. Vision Image Understanding **117**, 97–112 (2013).
23. F. Zhou, G. Zhang, and J. Jiang, "Constructing feature points for calibrating a structured light vision sensor by viewing a plane from unknown orientations," Opt. Lasers Eng. **43**, 1056–1070 (2005).
24. R. Yang, S. Cheng, W. Yang, and Y. Chen, "Robust and accurate surface measurement using structured light," IEEE Trans. Instrum. Meas. **57**, 1275–1280 (2008).
25. R. D. Wedowski, G. A. Atkinson, M. L. Smith, and L. N. Smith, "A system for the dynamic industrial inspection of specular freeform surfaces," Opt. Lasers Eng. **50**, 632–644 (2012).
26. Z. Zhang, "A flexible new technique for camera calibration," IEEE Trans. Pattern Anal. Mach. Intell. **22**, 1330–1334 (2000).
27. V. Lepetit, F. Moreno-Noguer, and P. Fua, "Epnp: an accurate o (n) solution to the PnP problem," Int. J. Comput. Vision **81**, 155–166 (2009).
28. I. S. Gradshteyn and I. M. Ryzhik, *Table of Integrals, Series, and Products* (Academic, 2014).
29. P. J. Best and N. D. McKay, "A method for registration of 3-d shapes," IEEE Trans. Pattern Anal. Mach. Intell. **14**, 239–256 (1992).
30. S. Rusinkiewicz, O. Hall-Holt, and M. Levoy, "Real-time 3d model acquisition," in *ACM Transactions on Graphics (TOG)* (ACM, 2002), vol. **21**, pp. 438–446.